# An enhanced motorcycle tyre model characterised through experimental riding data

# An enhanced motorcycle tyre model characterised through experimental riding data

Journal Title
XX(X):1–18

DOI: 10.1177/ToBeAssigned
www.sagepub.com/
SAGE

**Mirco Bartolozzi[1], Matteo Massaro[2], Matteo Mottola[2] and Giovanni Savino[1]**



**Abstract**

Tyre-road interaction governs motorcycle dynamics; however, the most widespread tyre model formulations must be characterised through a dedicated test bench on the lab or road, unavailable to many interested subjects.

This article proposed a new tyre model formulation, conceived to be characterised through riding data using standard instrumentation. Albeit its coefficients are identified through quasi-static, uncombined slip manoeuvres, the model addresses transient, combined manoeuvres and is adaptive to road friction levels and static weight through statistical relationships from the literature.

A pre-existing formulation was improved and expanded. The model's behaviour in demanding conditions was investigated through a high-fidelity simulation environment, using a Magic Formula tyre model as the reference. Next, the characterisation procedure was carried out using actual riding data. The model's accuracy is shown by reproducing numerically one of the manoeuvres and through comparison with the results of a bench test.

The proposed model could correctly reproduce the primary behaviour of a Magic Formula model, also concerning tyre moments and steering torque. Characterising the tyre model through real riding data proved feasible, and its robust formulation limited the propagation of estimation errors.

The proposed tyre model formulation and characterisation procedure should interest, among others, those subjects that lack access to a tyre testing machine.

**Keywords**

Motorcycle Tyre, PTWs dynamics, experimental validation, tyre model formulation, estimation of tyre forces and moments, slip angle estimation

## Introduction

Tyre-road interaction produces most of the forces and moments applied to road vehicles, governing their dynamics and handling.[1] Tyre behaviour determines the vehicle response and stability even when far from friction limits.[2,3] The primary importance of tyres concerning vehicle models used for diverse tasks (design and tuning of vehicles, tyres, and assistance systems, state estimation, handling and human-vehicle interaction) calls for an accurate and comprehensive description of their properties.

Two-wheeled vehicles, such as Powered Two-Wheelers or bicycles, are no exception.[4,5] Not only is their behaviour largely influenced by tyre slip; being tilting vehicles, their dynamics feature large camber angles, which constitutes an additional generation mechanism for lateral forces and yaw moments.[6–10]

Several tyre model formulations have been developed to describe tyre behaviour; the different philosophies span from theory-derived models (like analytical brush models),[11] to entirely empirical models (as fitting test data by regression, employing no similarity methods),[12] and vastly differ in complexity,[13] from very straightforward and limited (as the one by Dugoff et al.)[14] to highly complex and detailed (MF-Tire/MF-Swift/FTire/CDTire).[12,15–17] In particular, the Magic Formula (MF) tyre model is a widely used semi-empirical model that can describe the nonlinear and complex behaviour typical of motorcycle tyres. The model has been

[1]Department of Industrial Engineering, University of Florence, Italy
[2]Department of Industrial Engineering, University of Padova, Italy

**Corresponding author:**
Mirco Bartolozzi, Department of Industrial Engineering, University of Florence, Via di Santa Marta 3, Florence, Italy
Email: mirco.bartolozzi@unifi.it

continuously expanded to improve its robustness, detail and adaptability; however, all its versions have been conceived to be characterised using a tyre test bench machine, either in labs or roads[9,10,18–20] which allows applying any combination of tyre input quantities (load, slip, camber) and measure the resulting outputs (forces and moments). These devices are unavailable to many subjects (academic and industrial research groups, suppliers) interested in having a realistic model of the tyres equipping a given vehicle. Very few tyre test bench machines can generate the large camber angles typical of riding a two-wheeler: examples are the University of Padua's rotating-disk bench for motorcycle tyres,[9] and Polytechnic University of Milan's test-rig for bicycle tyres[21]. These two devices don't measure the longitudinal force or slip, because they were created for characterisations aimed at stability tests for which lateral dynamics is dominant[22]. Characterising a tyre through a test bench is time-consuming; additionally, test benches of labs feature road surfaces (made by sandpaper or steel belts for technical reasons) often not representative of real roads, and a friction similarity approach must be used,[23] which will inevitably introduce approximation errors, especially when investigating conditions close to the friction limits.

Lugo et al. proposed a novel tyre model formulation for car tyres that can be characterised through a limited set of quasi-static manoeuvres.[24] The model was validated experimentally: it accurately described each tyre's lateral force and yaw moment, even during transient manoeuvres, thanks to a dedicated relaxation-length formulation. The approach required affordable, general-purpose equipment, such as an Inertial Measurement Unit (IMU) and a sensor measuring the steering angle. Expensive equipment like slip angle sensors and wheel force transducers was avoided:[25] wheel kinematics (slip angles) and dynamics (forces and moments) were estimated by solving an algebraic, simplified car model at each time instant, which also prevented the use of Kalman filters, which would add complexity and tuning time.

Bartolozzi et al. adapted this approach to two-wheelers, for which the camber produces a significant amount of the lateral forces and yaw moments.[26] The dynamics of motorcycle tyres also differ from that of car tyres because there is no lateral load transfer, and the toroidal shape of their cross-section produces a lateral displacement of the contact centre, influencing the vehicle's roll angle. That article described the peculiar tyre model formulation and the characterisation manoeuvres used and validated the approach using a high-fidelity simulated dataset. Tyre forces, moments, and slips were accurately reproduced: the straightforward and efficient approach proposed proved successful. The article indicated that the few signals acquired were sufficient to identify the tyre model coefficients, providing a lower bound to the modelling error. These results called for validating the approach using experimental data and extending the model to widen its scope and purpose. In a real test, the noise, drift, and offsets affecting signals, and the measurement error concerning vehicle properties like the centre of mass position could increase the error significantly, even though Lugo et al. showed that the approach preserves its accuracy well when using experimental data;[24] however, this was relative to cars, which have simpler kinematics. Additionally, even though the motorcycle tyre model proposed by Bartolozzi et al. described tyre behaviour in a detailed way (through a nonlinear formulation for longitudinal and lateral forces and the longitudinal and yaw moments, produced by both slips and camber)[26], it was still lacking a description of more general conditions: its formulation only concerned quasi-static, uncombined manoeuvres; moreover, it was not adaptive concerning road friction levels. Lastly, even in quasi-static conditions, the model overestimated the front overturning moment and underestimated the rear one, even though their sum was in line with the actual value.

Focusing on these gaps, the present article has two goals: 1)To extend the tyre model formulation by Bartolozzi et al. to make it adaptive to different road friction and static load values and able to describe combined and transient dynamics, improving the description of the tyre overturning moment too; 2)To include experimental data, validating it for real-world applications. The global aim is to obtain a tyre model formulation that can be characterised using riding data employing a limited set of sensors and quasi-static, uncombined manoeuvres, which can reproduce both the primary input-output relationships (those between slip/camber and forces) and those secondary to steady-state motorcycle dynamics (moments), but essential for other aspects such as handling and stability. Although the characterisation tests are quasi-static, uncombined, and performed at specific road friction and static load values, the model must also reproduce transient, combined manoeuvres at different friction and static loads with acceptable accuracy through statistical relationships from the literature, whenever parameters are unavailable. Ideally, this model extension should require no additional tests compared to its first version to preserve its advantage over models to be characterised on the test bench.

The article is organised as follows. The general methodology, which includes simulated and real tests, is

laid out. The next section presents the proposed tyre model formulation, focusing on its peculiarities compared to more conventional tyre models. The following section concerns the simplified models for estimating additional signals and the general tyre characterisation procedure. Next, the results are shown by using a simulated dataset, assessing the model accuracy in demanding conditions, and the experimental test data. The characterisation results are shown for the latter dataset, and the model is validated concerning longitudinal dynamics using an intense braking manoeuvre and lateral dynamics by comparing the tyre model to the evidence from a bench test using the same tyres. The main findings and limitations are discussed, and their significance and future development are presented.

## General Methodology

The work consists of four steps:

1. *Model extension.* The previous tyre model formulation was extended to make it adaptive to different friction levels and static load values compared to the characterisation manoeuvres and to describe transient and combined dynamics conditions.
2. *Estimation models and characterisation procedure.* The simplified models used to estimate the quantities that are not directly measured (e.g. wheel forces) and the fitting process to estimate the tyre model were updated to make them more robust when using real data and to mirror the updates made to the tyre model.
3. *Simulated test*. Both this step and the following one contain a *characterisation* phase followed by a *validation* phase. The simulation environment allowed changing the test conditions arbitrarily and validating the tyre model using signals relative to tyre behaviour, which would be difficult to measure experimentally.
4. *Experimental test*. The characterisation procedure was tested experimentally to assess its feasibility and the corresponding fitting dispersion. The tyre model was then evaluated concerning critical aspects of tyre behaviour, like the longitudinal slip-force relationship and the cornering and camber stiffnesses, using bench test data as a reference. The experimental equipment is shown by Figure 1.

This work used the ISO 8855 signs convention (Figure 2):[27] the x-axis points forward, the y-axis leftward, and the z-axis upward. The reference frame is non-tilting. The rear tyre frame of reference coincides with that of the main frame. The front tyre reference frame can rotate around

**(a)** The instrumented motorcycle with outriggers. The positions of the steering angle sensor, inertial measurement unit, and wheel speed sensors are shown.

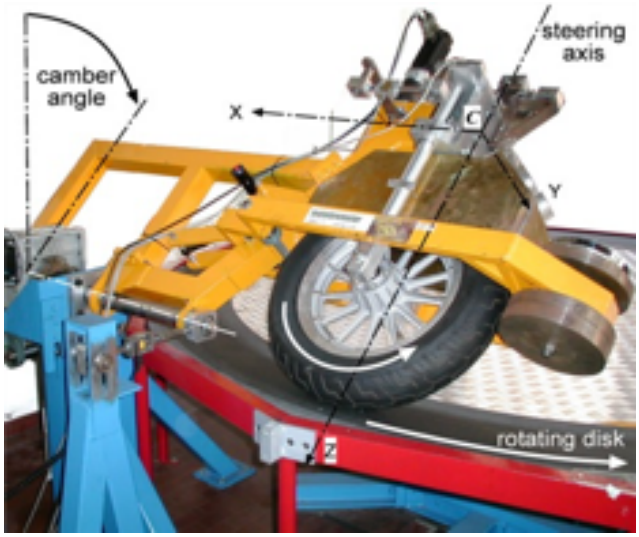


**(b)** Rotating-disk tyre test machine.

**Figure 1.** The equipment used.

the vertical axis with respect to that of the main frame. Notably, an anti-clockwise (when seen from above) slip angle is positive; in a left-hand corner, the camber angles are negative, and the lateral forces are positive. The notation used in the article is summarised in the Appendix.

## Tyre Model Formulation

### *General Characteristics*

The tyre model formulation describes four tyre outputs (the longitudinal force $F_x$, lateral force $F_y$, longitudinal moment $M_x$, and yaw moment $M_z$) based on four tyre inputs (the slip

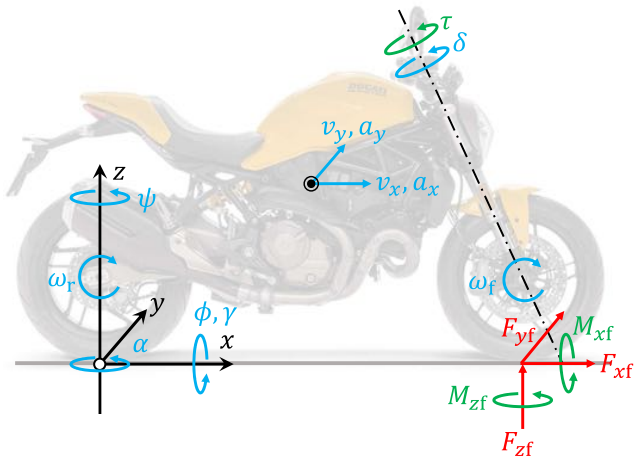


**Figure 2.** The signs convention and the main physical quantities considered in the article (each shown considering a positive value). Kinematic quantities are indicated in blue, forces in red, and moments in green. Tyre slip angle and camber are shown on the rear tyre, tyre forces and moments on the front tyre.

ratio $s$, slip angle $\alpha$, camber angle $\gamma$, and vertical force $F_z$) and one parameter (the road friction coefficient $\mu$*).

In a manoeuvre, many tyre inputs tend to vary together, especially in quasi-static manoeuvres: they are effectively *coupled*.[26] For example, in a front braking manoeuvre, the more intense the braking action, the higher the slip ratio of the front tyre and its vertical load (due to the load transfer): the slip ratio and the vertical load are coupled ($F_z = F_z(s)$). Analogous considerations apply to the slip and camber angles when cornering ($\alpha = \alpha(\gamma)$). This coupling makes it impossible to vary one tyre input without changing the other. A Magic Formula tyre model would be overfitted in a riding test as the low number of effectively independent inputs would not justify its numerous coefficients; a dedicated tyre model formulation is, therefore, required. By tailoring the tyre model to this specific application, the coupling is exploited to make the model more straightforward and more accurate as long as the dynamics don't evolve abruptly (e.g. road obstacles), as the influence of one variable is often taken implicitly into account in the variation of the other.

## Transient Behaviour

The delayed response of the tyre was modelled through a relaxation length formulation.[12] The dominant effect is the one related to the lateral response. The (lagged) slip angle $\alpha$ evolves as a first-order system:

$$d\alpha = \frac{v_{\tan}}{r_l} (\alpha_{\text{kin}} - \alpha)\, dt\,, \tag{1}$$

where the wheel's tangential speed $v_{\tan} = R_{\text{rol}}\omega$ is the product between its effective rolling radius $R_{\text{rol}}$ (constant in the model) and its spin angular speed $\omega$. The kinematic slip angle is computed as $\alpha_{\text{kin}} = \arctan(v_{sy}/v_x)$, where $v_x$ is the horizontal wheel speed component belonging to its midplane, and $v_{sy}$ is the slip speed component perpendicular to it. $r_l$ is the tyre relaxation length for lateral slip. No relaxation behaviour was considered for the longitudinal slip, for simplicity: $s = s_{\text{kin}} = v_{\tan}/v_x - 1$. No relaxation behaviour was considered for camber, too: $\gamma = \gamma_{\text{kin}}$.

## Slip Actions

Under combined slip conditions, the behaviour was managed through an adapted† version of Bakker's *Combined Slip Theory*,[28] which describes the behaviour of a tyre, characterised in conditions of road friction $\mu_0$, when the road friction assumes a generic value $\mu$. First, the theoretical longitudinal and lateral slip are computed from the practical slip quantities:

$$\sigma_x = -\frac{s}{1+s}\,, \tag{2a}$$

$$\sigma_y = -\frac{\tan\alpha}{1+s}\,, \tag{2b}$$

as the former is much more physically meaningful, and they are almost equal only when the longitudinal slip is small[29].

Then, the normalised slip components are obtained as

$$\sigma_x^* = \frac{\sigma_x}{\sigma_x^{\max}}\,, \tag{3a}$$

$$\sigma_y^* = \frac{\sigma_y}{\sigma_y^{\max}}\,, \tag{3b}$$

where $\sigma_{x,y}^{\max}$ are the slip values corresponding to the peak of the longitudinal and lateral slip force, respectively. Therefore, the peak slip force will be produced by a unitary normalised slip component. The total normalised slip is

$$\sigma^* = \sqrt{\sigma_x^{*2} + \sigma_y^{*2}}\,. \tag{4}$$

The total normalised slip and theoretical slip components are used to compute the equivalent longitudinal and lateral slips

$$s' = -\frac{\sigma^* \sigma_x^{\max} \operatorname{sign}\sigma_x}{1 + \sigma^* \sigma_x^{\max} \operatorname{sign}\sigma_x}\,, \tag{5a}$$

$$\alpha' = -\arctan\left(\sigma^* \sigma_y^{\max} \operatorname{sign}\sigma_y\right). \tag{5b}$$

*$\mu$ (without subscripts) is effectively a 'friction factor', used as suggested by Pacejka to nonlinearly scale the input-output curves relative to different road conditions[12] p. 150

†The theory, defined for car tyres, had to be adapted to motorcycle tyres, for which the effect of camber cannot be considered just an offset. Moreover, the peculiar tyre model formulation used called for further changes.

The product between the equivalent slips and the friction coefficients ratio $\mu_0/\mu$ is used to obtain the positive-valued *corrected slip-force characteristics* from the *slip-force characteristics* $\hat{F}_x$ and $\hat{F}_{y\alpha}$ which relate each slip quantity to the corresponding steady-state force:[‡]

$$F_{x0} = \left|\hat{F}_x\left\langle F_z, \frac{\mu_0}{\mu}s'\right\rangle\right| = \left|\mu_x\left\langle\frac{\mu_0}{\mu}s'\right\rangle\right| F_z\,, \tag{6a}$$

$$F_{y\alpha 0} = \left|\hat{F}_{y\alpha}\left\langle F_z, \frac{\mu_0}{\mu}\alpha'\right\rangle\right| = k_\alpha\left\langle\frac{\mu_0}{\mu}\gamma\right\rangle F_z\,|\alpha'|\,. \tag{6b}$$

The corrected slip-force characteristics are then modified to account for the anisotropic properties of the tire-road friction, obtaining the *basic curves*[28]:

$$F^*_{x0} = F_{x0} - \Gamma(F_{x0} - F_{y\alpha 0})\left(\frac{\sigma^*_y}{\sigma^*}\right)^2, \tag{7a}$$

$$F^*_{y\alpha 0} = F_{y\alpha 0} - \Gamma(F_{y\alpha 0} - F_{x0})\left(\frac{\sigma^*_x}{\sigma^*}\right)^2, \tag{7b}$$

where $\Gamma = \min(\sigma^*, 1)$. Lastly, the longitudinal and lateral slip force components are obtained:

$$F_x = -\cos(\lambda)\frac{\mu}{\mu_0}F^*_{x0}\operatorname{sign}\sigma^*_x\,, \tag{8a}$$

$$F_{y\alpha} = \sin(\lambda)\frac{\mu}{\mu_0}F^*_{y\alpha 0}\,, \tag{8b}$$

where $\lambda$ is the angle between the resulting slip force and the wheel's longitudinal direction. The transition of $\lambda$ from the normalised slip direction (forming an angle $\eta$ concerning the longitudinal direction) relative to small slip values to the slip direction (forming an angle $\theta$ concerning the longitudinal direction) relative to higher slip values is controlled by a coefficient ($\mathrm{q}_1$):

$$\lambda = \eta + \frac{2}{\pi}(\theta - \eta)\arctan\left(\mathrm{q}_1\sigma^{*2}_x\right), \tag{9a}$$

$$\eta = \arctan\frac{\sigma^*_y}{|\sigma^*_x|}\,, \tag{9b}$$

$$\theta = \arctan\frac{\sigma_y}{|\sigma_x|}\,. \tag{9c}$$

Friction similarity and combined slip theory were also used to compute the other forces and moments applied by the tyre. The yaw moment produced by the slip is

$$M_{z\alpha} = -t_\mathrm{p}\left\langle F_z, \frac{\mu_0}{\mu}\alpha'\right\rangle F_{y\alpha}\,, \tag{10}$$

where the pneumatic trail $t_\mathrm{p}$ is expressed by

$$t_\mathrm{p} = t_{\mathrm{p}0}\langle F_z\rangle\left(1 - \frac{k_{\alpha 0}}{3\mu}|\tan\alpha'|\right), \tag{11}$$

where $k_{\alpha 0}$ is the non-dimensionalised cornering stiffness (the cornering stiffness per unit of vertical load) evaluated in null slip and camber conditions. The pneumatic trail for vanishing slip, $t_{\mathrm{p}0}$, depends on vertical load:

$$t_{\mathrm{p}0} = t_\mathrm{p}\Big|_{\alpha'=0} = \frac{1}{3}\sqrt{R^2_\mathrm{unl} - R^2_\mathrm{loa}}\,, \tag{12a}$$

$$R_\mathrm{loa} = R_\mathrm{unl} - \frac{F_z}{K_z}\,, \tag{12b}$$

where the vertical tyre stiffness $K_z$ is constant.

## Camber Actions

In the model, tyre camber is responsible for an additional component of lateral force and yaw moment and for the overturning moment. Specifically, a force or moment component is added to the value determined from the combined slip equations, whose form was analogous[§] to that shown by Pacejka and Sharp[23]; these additional components decay with increasing slip. The camber actions are additive in the model; as such, they do not alter the previously described slip actions: the longitudinal force $F_x$ (Equation (8a)) does not depend on camber, and the lateral slip force $F_{y\alpha}$ (Equation (8b)) is influenced by camber only in the way already stated by Equation (6b).

For a tyre, the camber stiffness $K_\gamma$ is assumed to be proportional to its cornering stiffness $K_\alpha$ via a constant $C$ (*side force stiffness ratio*)[26]; the same holds when the two stiffnesses are expressed per unit of vertical load:

$$k_\gamma = Ck_\alpha\,. \tag{13}$$

Notice that, in this article, the cornering and camber stiffnesses are defined as the ratio between the steady-state lateral force and the angle causing it: this holds for any value of the angle and not just for its vanishing values. In the absence of longitudinal slip, the lateral camber force is

$$F^\mathrm{unc}_{y\gamma} = -K_\gamma\langle\gamma\rangle\gamma = -Ck_\alpha\langle\gamma\rangle F_z\gamma\,, \tag{14}$$

where 'unc' stands for 'uncombined'. Camber force decays with slip; however, the impact of lateral slip is already taken into account implicitly in the $k_\alpha\langle\gamma\rangle$ function, as the camber and slip angles are coupled when the tyre is characterised

[‡] In this article, angle brackets indicate the argument of a generic function describing tyre behaviour.

[§] Even though the form is analogous, the camber angle does impact the longitudinal and slip forces produced by the proposed tyre model, differently to the equations proposed by Pacejka and Sharp[23]. In fact, the camber angle is present in Equation (6b), and the resulting $F_{y\alpha 0}$ value influences the following equations up to Equations (8a) and (8b)

through steady state manoeuvres:[26] $k_\alpha\langle\gamma, \alpha\langle\gamma\rangle\rangle = k_\alpha\langle\gamma\rangle$. Consequently, only the longitudinal slip component is considered explicitly in the decay, whose rate is determined by a coefficient $\mathrm{c}_{Fy\gamma}$:

$$F_{y\gamma} = \frac{F_{y\gamma}^{\mathrm{unc}}}{1 + \mathrm{c}_{Fy\gamma}(\sigma_x^*)^2}\,. \tag{15}$$

Based on theoretical models[7,30] and experimental evidence,[18,30–32] the yaw moment produced by camber, often called *twisting moment*,[6,32] is approximately proportional to both camber and tyre load, via a coefficient $k_t$ denoted as 'non-dimensionalised twist stiffness':

$$M_{z\gamma}^{\mathrm{unc}} = -k_t F_z \gamma\,. \tag{16}$$

In the presence of slip, its value decreases (based on the $\mathrm{c}_{Mz\gamma}$ coefficient):

$$M_{z\gamma} = \frac{M_{z\gamma}^{\mathrm{unc}}}{1 + \mathrm{c}_{Mz\gamma}(\sigma^*)^2}\,. \tag{17}$$

The model includes an overturning moment $M_x$. The model considers a lenticular tyre. In reality, while cornering with a toroidal tyre, the ground contact point rolls over the minor torus circle; this displacement does not take place if the tyre is modelled as a thin disk, which would lead to a smaller roll angle. An overturning moment addresses that:

$$M_x = k_x F_z \tan\gamma\,, \tag{18}$$

where $k_x \tan\gamma$ is the moment arm for the vertical force acting on the tyre, so $k_x$ (non-dimensionalised overturning stiffness) is the radius of the minor torus circle deformed under the static load.

In the presence of a longitudinal force, the lateral $k_x \tan\gamma$ displacement will also produce the yaw moment

$$M_{zs\gamma} = k_x F_x \tan\gamma\,. \tag{19}$$

The total yaw moment is the sum of its three components:

$$M_z = M_{z\alpha} + M_{z\gamma} + M_{zs\gamma}\,. \tag{20}$$

### Rolling Resistance

Rolling resistance is considered proportional to tyre load and independent of speed:[30]

$$F^{\mathrm{rol}} = -c_{\mathrm{rol}} F_z\,, \tag{21}$$

where $c_{\mathrm{rol}}$ is the dimensionless rolling resistance coefficient of the tyre.

### Special Simplified Case

In the case of uncombined dynamics and friction equal to reference ($\mu = \mu_0$), the model simplifies to the version described and validated by Bartolozzi et al. in a previous article:[26]

$$F_x\left\langle s, F_z\right\rangle = \mu_x F_z\,, \tag{22a}$$
$$F_y\left\langle \alpha, \gamma, F_z\right\rangle = -k_\alpha F_z(\alpha + C\gamma)\,, \tag{22b}$$
$$M_x\left\langle \gamma, F_z\right\rangle = k_x F_z \tan\gamma\,, \tag{22c}$$
$$M_z\left\langle \alpha, \gamma, F_z\right\rangle = (t_{\mathrm{p}} k_\alpha \alpha - k_z\gamma)\, F_z\,, \tag{22d}$$
$$\mu_x = \mu_x\left\langle s\right\rangle\,, \quad k_\alpha = k_\alpha\left\langle\gamma\right\rangle\,, \quad t_{\mathrm{p}} = t_{\mathrm{p}}\left\langle\alpha\,, F_z\right\rangle\,. \tag{22e}$$

The only difference is that the slip angle $\alpha$ is the relaxed one instead of that computed kinematically.

## Estimation Models and Fitting

To be used, the tyre model must be *characterised*, meaning that the coefficients and functions that constitute its formulation must be determined.

### Assumed Quantities

Some coefficients are assumed a priori, based on either rules of thumb (the relaxation length $r_1$ and the $\mathrm{c}_{Fy\gamma}$ and $\mathrm{c}_{Mz\gamma}$ coefficients), prior evidence (the slip transition coefficient $\mathrm{q}_1$), or statistical evidence (the non-dimensionalised twisting stiffness $k_t$ and the side force stiffness ratio $C$).

The relaxation length $r_1$ (Equation (1)) was set equal to the wheel radius, following Pacejka's rule of thumb;[12] this approach had already been validated concerning the description of car tyres transient dynamics, using experimental data.[24] The slip transition coefficient $\mathrm{q}_1$ (Equation (9a)) was set to 1.1, as done by Bakker et al.[28]; if too high, the model might be less accurate for large slip, the opposite might hold if it is too low. Coefficients $\mathrm{c}_{Fy\gamma}$ (Equation (15)) and $\mathrm{c}_{Mz\gamma}$ (Equation (17)) should preferably be fitted to data from combined test bench data for that specific tyre. BikeSim's tyre documentation states, 'if combined test data is unavailable, a value of 1.0 is suggested': this value was used for the tyre model. The front and rear values for the non-dimensionalised twisting stiffness $k_t$ (Equation 16) were derived from the experimental data from several sources in the literature.[9,10,12,30,33] In particular, the value for the front and that for the rear tyre was computed as the average of the values relative to analogous tyres, as was done in the previous work by Bartolozzi et al.[26] In total, six front (120-70-R17) and three rear (180-55-R17) supersport

tyres were considered. The side force stiffness ratio $C$ (Equation (13)) for the front and rear tyres was obtained statistically, considering the tyre bench test data available in the literature.[9,20,34] The rationale follows: even though different tyres, operating under different load conditions, will have different cornering stiffness values, the variability will decrease when the cornering stiffness is evaluated per unit of vertical load acting on the tyre ('non-dimensionalised'), as the cornering stiffness is approximately proportional to the load up to moderate vertical force values.[12]. The same holds for camber stiffness. As the $C$ coefficient is defined as the ratio between the non-dimensionalised camber and cornering stiffnesses, its variability (and, therefore, the error introduced by assuming a statistically derived value) will be even lower if the cornering and camber stiffnesses for each tyre are positively correlated. Figure 3 shows the $k_\alpha$ and $k_\gamma$ values for different tyres, grouped by type. The values derived from the tyre test data in the previously mentioned articles.[9,20,34] The values for the 'Instrumented Motorcycle', used as a reference are an exception, as they consist of part of the results presented in the 'Results' section. The 'Premium Touring' tyre set (triangle markers) was characterised by low $k_\alpha$ and modest $k_\gamma$ values. The front and rear supersport tyres (circle markers) and the scooter tyres (square markers) had similar $k_\gamma$ values, while the rear supersport tyres had higher $k_\alpha$ values on average than the corresponding front tyres. The properties of the tyres equipping the instrumented motorcycle, which were excluded from the statistical analysis, are indicated as circle outlines. The correlation between the non-dimensionalised cornering and camber stiffness values was moderate-strong (0.59) when considering all the tyres, moderate (0.40) among the front supersport tyres (whose properties had modest deviation, though), and moderate-strong (0.60) among the rear supersport tyres. The $C$ value for the front and rear sport tyres was obtained by fitting Equation (13) to the ($k_\alpha$, $k_\gamma$) pairs. The $C$ value obtained for the front tyre (0.095) is close to the real one for the instrumented motorcycle (0.084); instead, the difference is significant concerning the rear tyres (0.078 vs. 0.129): the rear tyre equipping the instrumented motorcycle has an unusually high camber stiffness.

## Estimated Signals and Quantities

Some signals, like the slip angle or the tyre forces, cannot be measured accurately with cost-effective equipment; therefore, they were estimated at each sampling time by solving an algebraic, simplified motorcycle model, which includes some of the equations of the proposed tyre model relative to uncombined slip, quasi-static conditions as the characterisation manoeuvres. The process is discussed in additional detail in the previous work by Bartolozzi et al.,[26] and is summarised and updated in this section.

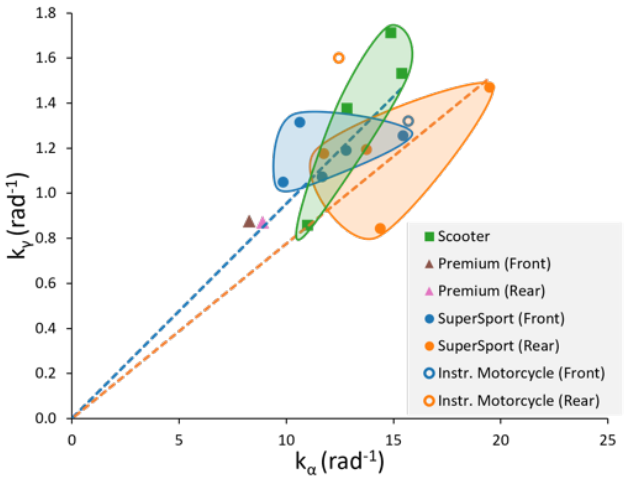


**Figure 3.** Cornering and camber stiffness per unit of vertical load for three different tyre types. The tyres equipping the experimental motorcycle are shown as circle outlines.

*Longitudinal dynamics* The front and rear effective rolling radii $R_{\text{rol}}$ and the dimensionless rolling resistance coefficient $c_{\text{rol}}$ are obtained from coasting manoeuvres. The effective rolling radius is estimated by fitting the $v_x = R_{\text{rol}}\omega$ equation to the $(\omega, v_x)$ pairs. The dimensionless rolling resistance coefficients are assumed to be the same front and rear, as it is impossible to discern between the front and rear rolling resistance contributions when observing the vehicle deceleration. The value of $c_{\text{rol}}$ is obtained by fitting the equation

$$ma_x = -c_{\text{drag}} v_x^2 - c_{\text{rol}} mg\,, \tag{23}$$

where $m$ is the motorcycle-rider mass (vertical aerodynamic forces are neglected), to the $(v_x, a_x)$ pairs; at the same time, $c_{\text{drag}}$ is obtained. The drag force signal can then be reconstructed as $F_{\text{drag}} = -c_{\text{drag}} v_x^2$.

The tyre slip ratio signal is computed using its SAE definition:

$$s = \frac{\omega R_{\text{rol}} - v_x}{v_x}\,. \tag{24}$$

A simple load transfer model, for which the pressure centre coincides with the centre of gravity, allows estimating the wheel loads as[26]

$$F_{z\text{f,r}} = mg\frac{l_{\text{r,f}}}{l} \mp \Delta F_z\,, \tag{25a}$$

$$\Delta F_z = (ma_x - F_{\text{drag}})\frac{h_{\text{G}}\cos\phi}{l}\,, \tag{25b}$$

where $h_{\text{G}}$ is the centre of mass height, $l$ is the wheelbase, which is divided by the longitudinal centre of mass position into the two parts $l_{\text{f,r}}$, and $\phi$ is the roll angle. Each tyre's

longitudinal force is estimated as

$$F_{x_\mathrm{r}} = \begin{cases} \rho\big(ma_x - F_\mathrm{drag} - (F_\mathrm{f}^\mathrm{rol} + F_\mathrm{r}^\mathrm{rol})\big) & \text{braking} \\ \quad + F_\mathrm{f}^\mathrm{rol} & \\ F_{\mathrm{rol_f}} & \text{otherwise} \end{cases} \tag{26}$$

$$F_{x_\mathrm{r}} = \begin{cases} (1-\rho)\big(ma_x - F_\mathrm{drag} & \\ \quad - (F_\mathrm{f}^\mathrm{rol} + F_\mathrm{r}^\mathrm{rol})\big) + F_\mathrm{r}^\mathrm{rol} & \text{braking} \\ ma_x - (F_\mathrm{drag} + F_{\mathrm{rol_f}}) & \text{otherwise} \end{cases} \tag{27}$$

where $\rho$ is the brake balance ($\rho = 0$: rear braking, $\rho = 1$: front braking). Lastly, the estimated coefficient of engaged longitudinal friction $\mu_x$ is computed as the ratio between the estimated longitudinal and vertical force acting on the tyre.

The function $\mu_x\langle s\rangle$ (Equation (6a)) relating the slip ratio $s$ to the longitudinal friction $\mu_x$ produced is obtained by fitting a simplified, asymmetric[¶] version of the Magic Formula through braking and driving data, using the computed slip ratio as the independent variable:

$$\mu_x\langle s\rangle = d\sin\Big\{c\arctan\big[bs - (e_1 + e_2\operatorname{sign} s)(bs - \arctan(bs))\big]\Big\}, \tag{28}$$

obtaining its coefficients $b, c, d, e_1, e_2$. $\sigma_x^\mathrm{max}$ is then found numerically, after restating the Equation (28) in terms of $\sigma_x$. For each tyre, $\sigma_y^\mathrm{max}$ is assumed to be equal to $\sigma_x^\mathrm{max}$.

*Lateral dynamics* The front and rear slip angles are estimated through a single-track model:[26]

$$\alpha_\mathrm{f} = \frac{v_{y_\mathrm{G}} + h_\mathrm{G}\cos\phi\dot{\phi} + l_\mathrm{f}\dot{\psi}}{v_x} - \Delta\,, \tag{29a}$$

$$\alpha_\mathrm{r} = \frac{v_{y_\mathrm{G}} + h_\mathrm{G}\cos\phi\dot{\phi} - l_\mathrm{r}\dot{\psi}}{v_x}\,, \tag{29b}$$

where $v_{y_\mathrm{G}}$ is the lateral speed of the centre of mass, $\dot{\psi}$ is the yaw rate, and $\Delta$ is the kinematic steering angle, computed as

$$\Delta = \arctan\left(\frac{\sin\delta\cos\epsilon}{\cos\phi\cos\delta - \sin\phi\sin\delta\sin\epsilon}\right), \tag{30}$$

where $\delta$ and $\epsilon$ are the steering angle at the handlebars and the caster angle. The camber angles are computed as:

$$\gamma_\mathrm{f} = \arcsin\left(\cos\delta\sin\phi + \cos\phi\sin\delta\sin\epsilon\right), \tag{31a}$$

$$\gamma_\mathrm{r} = \phi\,. \tag{31b}$$

The lateral forces are estimated as

$$\begin{pmatrix} F_{y_\mathrm{f}} \\ F_{y_\mathrm{r}} \end{pmatrix} = \begin{bmatrix} l - \tilde{t}_{\mathrm{p_f}} & -\tilde{t}_{\mathrm{p_r}} \\ \tilde{t}_{\mathrm{p_f}} & l + \tilde{t}_{\mathrm{p_r}} \end{bmatrix}^{-1} \begin{pmatrix} l_\mathrm{r} m\dot{\psi}v_x - M_{z_{\gamma_\mathrm{f}}} - M_{z_{\gamma_\mathrm{r}}} - M_{z_\mathrm{long}} \\ l_\mathrm{f} m\dot{\psi}v_x + M_{z_{\gamma_\mathrm{f}}} + M_{z_{\gamma_\mathrm{r}}} + M_{z_\mathrm{long}} \end{pmatrix}, \tag{32}$$

where

$$\tilde{t}_{p_{\mathrm{f,r}}} = \frac{\alpha_{\mathrm{f,r}}}{\alpha_{\mathrm{f,r}} + C_{\mathrm{f,r}}\gamma_{\mathrm{f,r}}} t_{p_{\mathrm{f,r}}}\,, \tag{33a}$$

$$M_{z_\mathrm{long}} = -h_\mathrm{G}\sin\phi(ma_x - F_\mathrm{drag})\,, \tag{33b}$$

and $M_{z_{\gamma_{\mathrm{f,r}}}}$ are computed using Equation (16).

The front and rear non-dimensionalised overturning stiffness coefficient $k_{x\mathrm{f,r}}$ (Equation (18)) must be estimated. The total overturning moment is estimated by comparing the measured roll angle ($\phi$) with the one ($\phi_\mathrm{len}$) a motorcycle with lenticular tyres would have, in steady-state, under the same lateral acceleration:

$$M_x^\mathrm{tot} = mh_\mathrm{G}\big[\dot{\psi}v_x(\cos\phi_\mathrm{len} - \cos\phi) - g(\sin\phi_\mathrm{len} - \sin\phi)\big]\,, \tag{34a}$$

$$\phi_\mathrm{len} = -\arctan\frac{\dot{\psi}v_x}{g}\,. \tag{34b}$$

Then, the $(\phi, M_x^\mathrm{tot})$ pairs relative to quasi-static corners are fitted through the following equation, obtaining the $k_x$ coefficient:

$$M_x^\mathrm{tot} = k_x F_z\tan\phi\,, \tag{35}$$

which is used just to compute each tyre's non-dimensional overturning stiffness:

$$k_{x\mathrm{f}} = \frac{mg}{F_{z\mathrm{f}} + F_{z\mathrm{r}} r_\mathrm{f}/r_\mathrm{r}} k_x\,, \tag{36a}$$

$$k_{x\mathrm{r}} = \frac{r_\mathrm{f}}{r_\mathrm{r}} k_{x\mathrm{f}}\,, \tag{36b}$$

where $r_{\mathrm{f,r}}$ are the front and rear tyre widths. Differently from the previous formulation, the front and rear overturning stiffnesses are now distinct, and the ratio between the two is assumed to be the ratio between the tyre widths (Equation (36b)).

Now that the signals relative to the slip and camber angles and the tyre forces have been estimated, the function $k_\alpha\langle\gamma\rangle$ (Equation (6a)) relating the non-dimensional cornering stiffness to the camber angle can be characterised.

[¶] The asymmetry is necessary due to tyre load sensitivity, and the implicit impact of the vertical load on the longitudinal friction.

## Tests Conducted

### BikeSim Simulations

The simulations were conducted through the motorcycle simulation software BikeSim© (Mechanical Simulations, Ann Arbor, MI, US).[35] Its high-fidelity motorcycle models were equipped with a Magic Formula tyre model (5.2 version), in the version refined by Sharp,[33] which computed the tyre outputs (the longitudinal and lateral forces $F_{x,y}$ and the yaw moment $M_z$) from its inputs (the slip ratio $s$, slip angle $\alpha$, camber angle $\gamma$, and vertical force $F_z$). The Magic Formula model can describe tyre behaviour in combined slip conditions and for different friction levels and also models the outputs build-up during transients.

Two phases are performed:

1. In the *Characterisation phase*, the *Sports Small* motorcycle model (the same as in the previous study[26]) was employed in the quasi-static manoeuvres needed for the characterisation of the custom tyre model. The vehicle used the default Magic Formula tyres to proxy for real tyres. A coasting manoeuvre (running in neutral) was performed to estimate the tyres' rolling radii, rolling resistance coefficients, and aerodynamic drag coefficients. Front and rear braking manoeuvres, with the transmission in neutral position and intensity increasing progressively from zero to wheel lock, characterised the negative side of the slip ratio-longitudinal force relationship for each tyre. The rear tyre was also characterised by the effect of positive slip through a second-gear acceleration manoeuvre, where the throttle input increased progressively. Lateral dynamics was investigated through a decreasing-radius corner approached at constant speed: the motorcycle initially travelled straight and leaned gradually up to the grip limits. These simulations were performed using a unitary friction coefficient: $\mu_0 = 1$. The characterisation manoeuvres were analogous to those of the previous study;[26] the only difference was that they were conducted up to the friction limits to explore the complete nonlinear behaviour of the tyres.
2. In the *Validation phase*, a different motorcycle model (*Sports Touring*) model was used to perform a transient, combined manoeuvre in conditions of lower grip ($\mu = 0.75$). The scope of this phase was to assess whether the proposed tyre model and characterisation procedures allowed describing a manoeuvre having friction levels, dynamics (transient instead of quasi-static, combined instead of uncombined), and static load values different compared to those used in the characterisation procedure. The manoeuvre was executed twice: in the first instance, the 'Sports Touring' motorcycle employed the same Magic Formula tyre model used in the characterisation phase (where it had equipped the 'Sports Small' motorcycle); in the second, it was fitted with the custom tyre model characterised in the previous phase. The custom tyre model was implemented in MATLAB-Simulink©, and it received the tyre input signals from the BikeSim motorcycle model. Including the rider and compared to the 'Sports Small' motorcycle, the 'Sports Touring' motorcycle had a higher mass ($308\,\mathrm{kg}$ vs. $260\,\mathrm{kg}$, +18.4%) and a more frontward mass distribution (53.1% vs. 49.7%) compared to the other. The manoeuvre was a lane change having a $3\,\mathrm{m}$ lateral offset and a $20\,\mathrm{m}$ transition distance, the same as the lane change considered by Cossalter and Sadauckas for a touring motorcycle.[36] The speed controller generated the speed profile that minimised the time required to manoeuvre the following performance envelope constraints:[37] $2.5\,\mathrm{m\,s^{-2}}$ maximum positive longitudinal acceleration, $5.0\,\mathrm{m\,s^{-2}}$ maximum negative longitudinal acceleration, and $6.0\,\mathrm{m\,s^{-2}}$ maximum lateral acceleration. A friction ellipse was generated using these values and limited the combination of the two orthogonal acceleration components when both were present. Notice that the maximum acceptable acceleration ($0.61\mathrm{g}$) was not far from what was allowed by the friction coefficient used. Braking was performed with a fixed brake balance (60% front). A feed-forward PID for path tracking generated the steering input.

### Experimental Test

An experimental test was conducted using an instrumented sports, naked motorcycle (Figure 1a). An inertial measurement unit (XSens 680 Gi), installed on the tank with a GNSS antenna on the tail, provided the velocity vector, the acceleration vector, and the Euler angles describing the vehicle's orientation. A rotary potentiometer (TPS280DP) measured the steering angle, and the OEM wheel speed sensors provided each wheel's angular speed around its spindle axis. A pair of lightweight outriggers allowed safely reaching high lean angles ( $40°$). An experienced rider performed the tests; the ABS was set to the least conservative intervention threshold ('Sport Mode'). The primary motorcycle parameters were either known (e.g. the caster angle) or measured; in particular, the longitudinal position of the motorcycle-rider centre of mass was obtained by weighting the system through two weighting scales; its height was computed by using the

readings of an additional weighting performed at an angle, through the approach described by Cossalter.[32]

The experimental test was conducted in a closed-to-traffic test area and was divided into the same two phases as the tests conducted through BikeSim:

1. *Characterisation Phase*. The rider performed 16 coasting manoeuvres: eight of them started at around $20\,\mathrm{km\,h^{-1}}$; eight started at around $50\,\mathrm{km\,h^{-1}}$ and ended at around $35\,\mathrm{km\,h^{-1}}$. Each group of eight runs consisted of four runs in each direction to compensate for the effect of any wind or slope. Next, six front braking manoeuvres were performed starting from around $70\,\mathrm{km\,h^{-1}}$, where the rider progressively increased the braking pressure up to the friction limits. The rider then performed six analogous braking manoeuvres using the rear brake. The rider started from a standstill and accelerated in first gear, progressively opening the throttle to the maximum. Then, he put the gearbox in neutral, waited for the vehicle to stabilise, and started to brake. One of the six front braking manoeuvres was used to validate the tyre model; as such, it was excluded from the characterisation dataset. Concerning lateral dynamics, the rider performed 20 laps of a course consisting of two left-hand corners (with centre line radii equal to $12.5\,\mathrm{m}$ and $15\,\mathrm{m}$) connected by two short straights. The rider made the motorcycle lean progressively in and out of each corner, slowly enough to make the manoeuvre quasi-static. The rider leaned together with the motorcycle to make the manoeuvre more repeatable; moreover, he was instructed not to use the brakes or the throttle during the cornering sections (uncombined dynamics).
2. *Validation phase*. A model resembling the instrumented motorcycle was created in BikeSim using the known parameters. Once again, the custom tyre model was implemented in MATLAB-Simulink using the coefficients identified in the characterisation phase. The relationship between the front braking pressure and the corresponding deceleration was obtained through linear regression of the experimental data; this relationship was used to set the friction coefficient of the front brake pad in the BikeSim model. A BikeSim simulation was then performed using the experimental front brake pressure signal as input, and the resulting simulated front wheel slip ratio was compared to that computed using experimental data. After the test, the University of Padua's rotating-disk tyre test machine (Figure 1b) was used to derive the tyres' properties.[9] The scope was to experimentally validate the tyre model concerning some key aspects of lateral dynamics. The tests were executed for each tyre with a vertical load equal to the static load of the instrumented motorcycle acting on that tyre. Three type of tests were conducted: *slip tests*, where the slip angle spanned from $-5°$ to $5°$ ($1°$ step) while the camber angle was null; *camber tests*, where the camber angle spanned from $-45°$ to $45°$ ($15°$ step) while the slip angle was null; *combined tests*, where all the combinations of slip (between $-3°$ to $3°$, $1°$ step) and camber (between $-30°$ to $30°$, $15°$ step) were tested. These data allowed comparing the tyre model's non-dimensionalised cornering and camber stiffness with the true values and the lateral friction coefficient produced by the tyre model with the one measured on the test bench.

## Results

### *BikeSim Simulations*

The results of the characterisation procedure are omitted, as they are analogous to those discussed in the previous article.[26] Figure 4 shows the results of the BikeSim simulation, which employs the 'Sports Touring' motorcycle model, that compares the default, reference tyre model (in grey) to the custom tyre model formulation (in black) whose coefficients were previously identified when both equipped the 'Sports Small' motorcycle model. Tyre signals relative to the front tyre are shown as solid lines, and those relative to the rear tyre are shown as solid lines with round markers.

The rider started the lane change at $1.4\,\mathrm{s}$, changed direction around $3.4\,\mathrm{s}$ and returned to straight riding at the end of the simulation. They braked with increasing intensity up to around $2.5\,\mathrm{s}$, then partially released the brake as they started cornering. After the apex of the second cornering section ($4.0\,\mathrm{s}$), the rider went on the throttle to exit the lane change quickly.

The results generally showed a strong agreement between the reference and custom tyre models. The steering torque $\tau$ and steering angle $\delta$ were well predicted, with a modest deviation between the two models: peak values were $-10.1\,\mathrm{N\,m}$ vs. $-11.3\,\mathrm{N\,m}$ (11.8% overestimated), and $0.77\,\mathrm{deg}$ vs. $0.74\,\mathrm{deg}$ (2.8% underestimated). Concerning tyre slip, the slip ratio $s$ produced by the custom tyre model followed that of the reference tyre closely: peak values for the rear tyre were $-0.071$ vs. $-0.067$ (6.3% underestimated) when braking, and $0.025$ vs. $0.024$ (3% underestimated) when using the throttle. Under braking, the

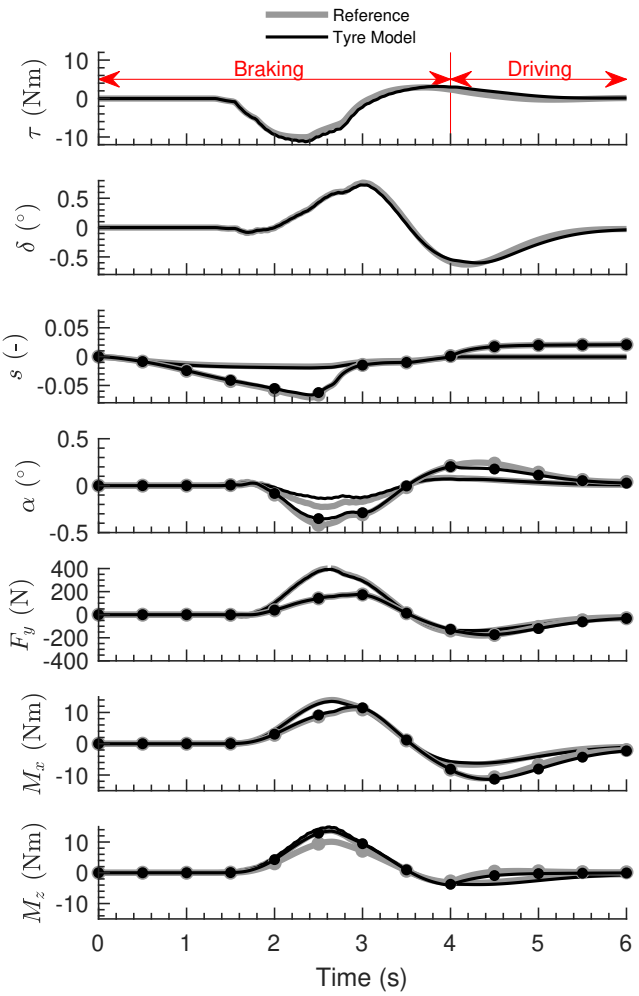


**Figure 4.** Motorcycle and tyre behaviour during the combined lane change manoeuvre. The reference tyre is grey, and the custom tyre model is black. Quantities relative to the rear tyre are shown as solid lines with round markers.

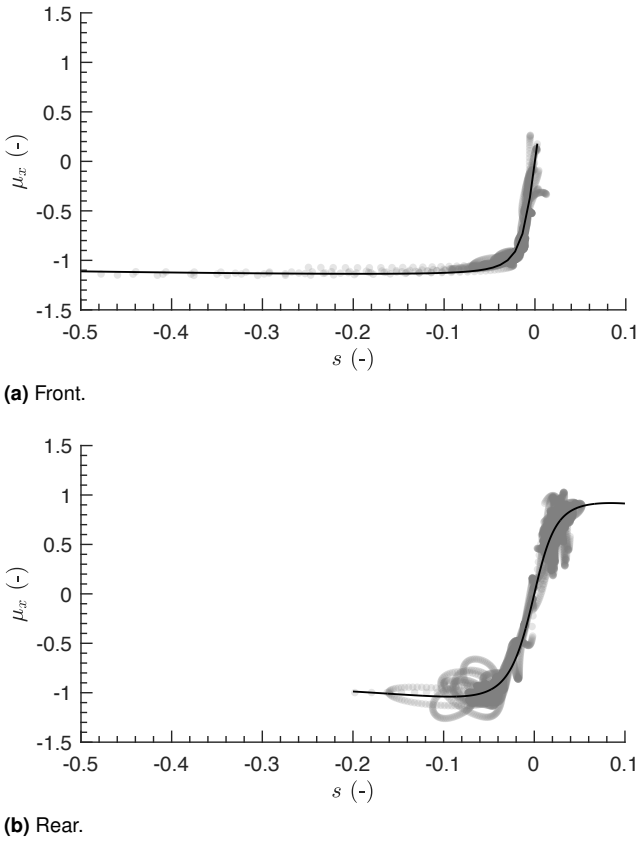


**(a)** Front.

**(b)** Rear.

**Figure 5.** Experimental data for longitudinal tyre dynamics, fitted through the Magic Formula (Equation (28)).

slip ratios on the front tyre were modest (peak values $-0.017$ vs. $-0.019$, $12.6\%$ overestimated) as the load transfer increased its grip significantly compared to the rear tyre. Slip angles $\alpha$ had a higher relative error, especially the front on corner entry ($-0.23\,\mathrm{deg}$ vs. $-0.15\,\mathrm{deg}$ peak values, $33.6\%$ underestimated). In general, slip angles were underestimated in all sections, even though the error on the rear tyre was less significant. The lateral force $F_y$ and overturning moment $M_x$ produced by each tyre showed a strong agreement between the reference tyre and the custom tyre model. Lastly, the yaw moment $M_z$ produced by the custom tyre model matched that of the reference tyre concerning the front tyre ($13.7\,\mathrm{N\,m}$ vs. $14.9\,\mathrm{N\,m}$ peak values, $8.8\%$ overestimated), while the error was higher on the rear tyre ($10.1\,\mathrm{N\,m}$ vs. $13.5\,\mathrm{N\,m}$ peak values, $34\%$ overestimated).

## *Experimental Test*

*Characterisation* In all the following regressions, robust bisquare weights fitting was used to make the result impacted less by outliers.[38] Results of fitting the $\mu_x\langle s\rangle$ function (Equation (28)) are shown in Figure 5. In particular, the rear tyre (Figure 5b) was fitted concerning both braking and driving; the peak coefficient of engaged longitudinal friction was slightly lower in the latter case, coherently with the phenomenon known as 'tyre load sensitivity'.[12] Some hysteresis was present when braking with the rear tyre due to ABS intervention induced by the load transfer. The dispersion around the fitting line was partly due to the many trials considered.

A regression was then performed to determine the steady-state relationship between the tyre camber angle and slip angle and the one between the camber angle and the corresponding coefficient of engaged lateral friction. The former was performed through the odd third-order polynomial

$$\alpha\langle\gamma\rangle = \mathrm{c}_1\gamma + \mathrm{c}_3\gamma^3\,, \tag{37}$$

while the latter was carried out through a tangent function, as suggested by the steady-state force balance:[32]

$$\mu_y\langle\gamma\rangle = \mathrm{c}_\mathrm{t}\tan\gamma\,. \tag{38}$$

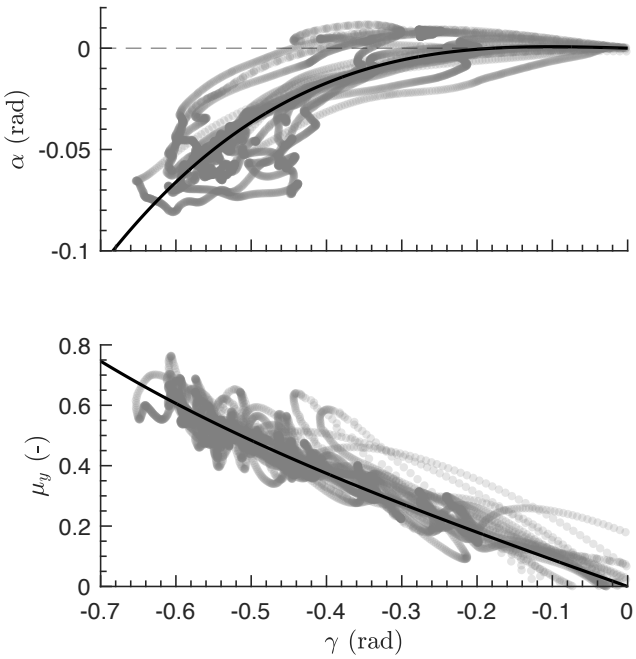


**Figure 6.** Experimental data for lateral tyre dynamics, fitted through appropriate functions (Equations (37) and (38)). The rear tyre is shown.

The two functions obtained were then used to compute the cornering stiffness function

$$k_\alpha\langle\gamma\rangle = \frac{\mu_y\langle\gamma\rangle}{\alpha\langle\gamma\rangle + C\gamma}\,. \tag{39}$$

Notice that fitting $\frac{\mu_y}{\alpha+C\gamma}\langle\gamma\rangle$ directly would produce numerical division by values approaching zero for small values of the denominator. This problem is present, to a low degree, even when using a simulated, noise-free dataset,[26] and worsens with experimental data. Instead, fitting the $\alpha\langle\gamma\rangle$ and $\mu_y\langle\gamma\rangle$ functions independently through functions defined to cross the axes' origin prevents the problem.

Figure 6 shows the regression for the rear tyre. One notices that, for small camber angles, the slip angle tended to be approximately null independently of the camber angle value: this means that the non-dimensionalised rear camber stiffness $k_\gamma$ assumed approximately unitary values, that is, the camber thrust was close to the force required to corner with the lateral acceleration associated to that motorcycle roll angle value.[9] For higher lateral acceleration values and, therefore, camber angles, the slip angle turned negative: in left-hand corners ($\gamma < 0$), the slip angle was clockwise ($\alpha < 0$); hence, the tyre tended to slide towards the outside of the corner. The camber force became insufficient to produce the required cornering force, and the tyre slipped to contribute additional force.

The estimated functions for the non-dimensionalised stiffnesses are shown by Figure 7. The upper subplot shows the cornering stiffnesses, while the camber stiffnesses are in the lower subplot. Solid lines and solid lines with markers are relative to the front and rear tyres, respectively. The values measured at the tyre test bench are also included as a grey triangle (front tyre) and square (rear tyre) as a reference. The characterised tyre model predicted a more significant decay in cornering and camber stiffnesses for the rear tyre than the front tyre as the camber angle (and, implicitly, the slip angle) increased. The estimated non-dimensionalised cornering stiffness for vanishing slip and camber $k_{\alpha 0}$ was $12.5\,\mathrm{rad}^{-1}$ for the front tyre (vs. the measured $15.7\,\mathrm{rad}^{-1}$, 21.4% underestimated), and $13.2\,\mathrm{rad}^{-1}$ for the rear tyre (vs. the measured $12.5\,\mathrm{rad}^{-1}$, 5.6% overestimated). The corresponding non-dimensionalised camber stiffnesses were $1.19\,\mathrm{rad}^{-1}$ (vs. the measured $1.32\,\mathrm{rad}^{-1}$, 9.8% underestimated), and $1.03\,\mathrm{rad}^{-1}$ (vs. the measured $1.60\,\mathrm{rad}^{-1}$, 35.6% underestimated). The error was higher on the rear tyre: as Figure 3 showed, the tyre had a higher $C = k_\alpha/k_\gamma$ ratio compared to analogous tyres found in the literature; this produced an overestimation of its cornering stiffness. However, in steady state, the tyre model formulation is such that using a $C$ value moderately different than the real one should not impact the slip angle produced by the model, as was shown in the previous article.[26] In fact, an infinite number of $(k_\alpha, k_\gamma)$ combinations will produce a given slip angle in a given cornering condition. Therefore, the error in the slip angle can be smaller than that on the cornering stiffness. Isolating the slip angle from Equation 22b, one gets

$$\alpha = -\frac{\mu_y\langle\gamma\rangle + k_\gamma\langle\gamma\rangle\gamma}{k_\alpha\langle\gamma\rangle} = -\frac{\mathrm{c_t}\tan\gamma + k_\gamma\langle\gamma\rangle\gamma}{k_\alpha\langle\gamma\rangle}\,, \tag{40}$$

which, for vanishing slip and camber angles, can be stated in terms of slip angle per unit of camber angle

$$\frac{\alpha}{\gamma} = -\frac{\mathrm{c_t} + k_{\gamma 0}}{k_{\alpha 0}}\,. \tag{41}$$

Substituting the $\mathrm{c_t}$ value obtained previously, one can compute this ratio using the estimated or the measured non-dimensionalised stiffnesses. For the front tyre, the ratio was equal to $0.0279$ (estimated) and $0.0305$ (measured), leading to the slip angle being underestimated $0.0026°$ for every degree of camber angle, which is extremely modest. For the rear tyre, the ratio equalled $0.0107$ (estimated) and $0.0574$ (measured): the slip angle was overestimated $0.0467°$ for every degree of camber angle, which was higher than the error on the front slip angle, as expected.

*Validation* Figure 8 shows the results concerning the front-braking manoeuvre considered. Signals measured, directly or

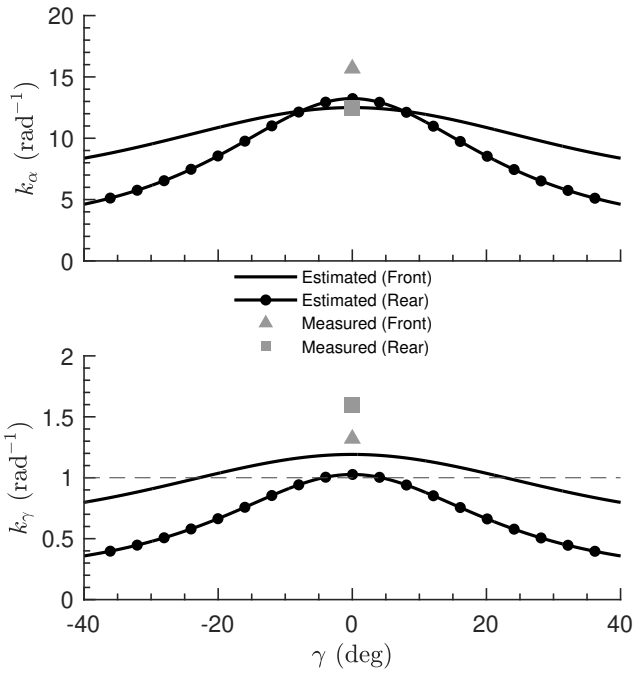


**Figure 7.** Estimated cornering and camber stiffnesses as an explicit function of camber. The values measured at the test bench, relative to vanishing slip and camber, are shown in grey.

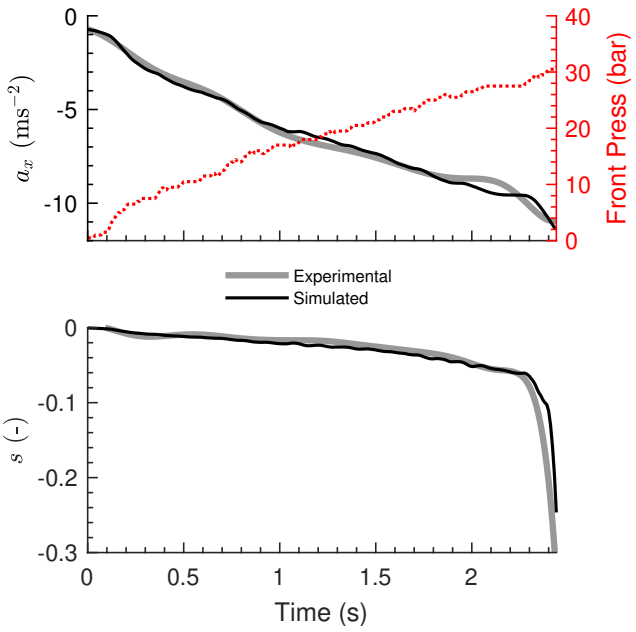


**Figure 8.** Measured versus simulated longitudinal acceleration and front tyre slip ratio during a front braking manoeuvre.

derived, are shown in grey; the simulation results are shown in black. The upper subplot shows the measured (grey) vs. simulated (black) longitudinal acceleration, and the lower subplot exhibits the slip ratio. The measured front braking pressure, the input for the simulation, is plotted as a dotted red line.

Until the longitudinal friction limit is reached, the longitudinal acceleration is dictated by the braking pressure requested by the rider. The linear fit of longitudinal acceleration for different front pressure values allowed for reproducing the vehicle's longitudinal acceleration properly. One notices good agreement between the measured and the simulated slip ratio. The tyre exhibited a more negative slip ratio in the simulation as the brake pressure increased, slightly overestimating the measured slip ratio. Notably, the custom tyre model started to show unstable behaviour (slip ratio increasing at an ever-increasing rate) around $2.3\,\mathrm{s}$ after the beginning of the manoeuvre, agreeing with the experimental data. Therefore, the custom tyre model correctly predicted the approaching of the friction limits conditions when the phenomenon manifests experimentally. When the simulation finished ($2.44\,\mathrm{s}$) the longitudinal acceleration was $-11.3\,\mathrm{m\,s^{-2}}$ and the slip ratio was $-0.246$; in the experimental data, this value was reached just $0.02\,\mathrm{s}$ sooner, producing a $-10.9\,\mathrm{m\,s^{-2}}$ acceleration. Therefore, the tyre model reproduced the approaching of longitudinal friction limits correctly. Figure 5a shows that, for the braking manoeuvres used in the characterisation, the fitting Magic Formula tended to slightly overestimate the grip produced in the $-0.08$ to $-0.25$ slip range: this explains the analogous behaviour in the simulation.

The final comparison between the characterised custom tyre model and the tyre properties measured on the bench test consisted of comparing the lateral force per unit of vertical load generated for a given slip and camber angle pair; the results are shown by Figure 9. ~~The measured coefficient of engaged lateral friction is shown as a coloured surface (dark blue indicates high and negative values and light green indicates high and positive values).~~ Differently than in a bench test, during steady-state manoeuvres, the slip and camber angles are coupled; therefore, the domain was explored using the previously identified $\alpha\langle\gamma\rangle$ function (Equation 37). The coefficient of engaged lateral friction of the custom tyre is shown as the height of parallel blue lines; the difference between measured and estimated values is represented as parallel red lines.

The results are shown for the rear tyre since it was affected by a higher error, as attested by the difference between the estimated and measured non-dimensionalised camber stiffnesses and as predicted by Equation 41. The relative error was very tiny for camber angle values up to $10°$ and was moderate up to around $20°$. For a given instant during a manoeuvre, the tyre's coefficient of engaged lateral friction will assume a specific value, and the equilibrium of the weight and centrifugal forces will determine the camber angle. Therefore, any difference between the measured and estimated coefficient will manifest as a difference in the slip angle obtained. Notice that, even though the

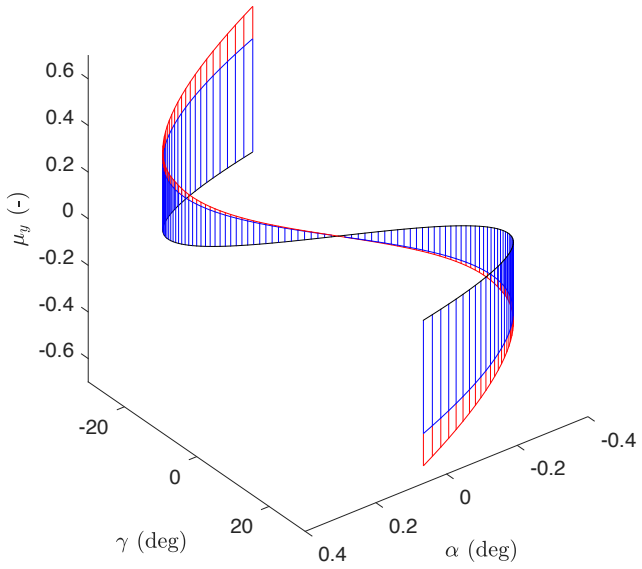


**(a)** Global view.

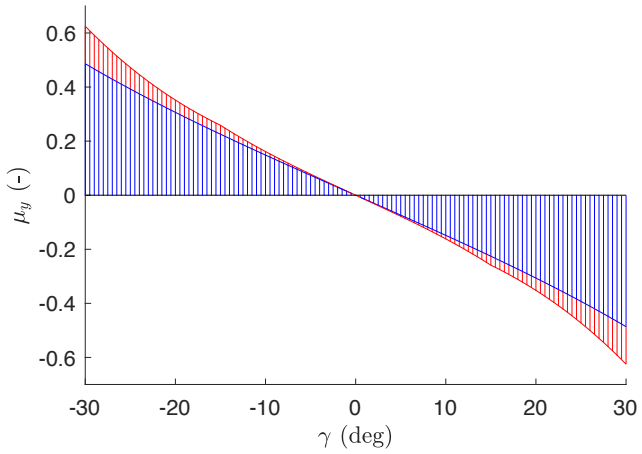


**(b)** Camber angle view.

**Figure 9.** Tyre model coefficient of lateral engaged friction as an explicit function of camber (height of the blue lines) versus that obtained through the bench test in the camber-slip domain ~~(coloured surface)~~. The difference between the two is in red. The results shown are relative to the rear tyre.

$\mu_y\langle\gamma,\alpha\rangle$ relationship represented by the coloured surface was obtained through linear interpolation of measured values, its value when expressed as an explicit function of camber $\mu_y\langle\gamma,\alpha\langle\gamma\rangle\rangle$ (the length of blue and red lines in Figure 9b) was nonlinear: the nonlinearity was introduced by the $\alpha\langle\gamma\rangle$ relationship (Equation 37).

## Discussion

A complete motorcycle tyre model formulation was defined and characterised through riding data. The physical readings of wheel speed sensors, an IMU, and a steering angle sensor were sufficient to identify the parameters of the tyre model proposed.

In the validation through the simulated dataset, the motorcycle model differed from that employed in the characterisation procedure (touring vs. sports). This choice was made to investigate whether the characterisation procedure would describe the tyres equipping the vehicle and not just the motorcycle-tyre system. In fact, the behaviour of tyres is influenced by the characteristics (e.g., mass and centre of mass position) of the vehicle employing them: a tyre model that describes tyre behaviour well independent of the vehicle it equips is more valuable and general. This goal was achieved, as attested by the following results. Overall, the custom tyre model reproduced the main features of a Magic Formula tyre model, and it was successfully characterised through the method proposed. This fact also held for some secondary aspects of motorcycle dynamics (e.g. the overturning moments). In particular, the steering torque, which has a prominent impact on handling,[36,39] was correctly reproduced; this attests to the correct description made by the proposed tyre model, as steering torque is significantly influenced by various aspects relative to tyre behaviour.[40] Coming to the slip angles, they were affected by a higher relative error compared to other signals; still, the absolute error was small and, more importantly, of the same sign for both tyres: this preserved the directional behaviour of the motorcycle, as confirmed by the steering angle signal departing minimally from that of the motorcycle employing the reference tyre model. The slip angle underestimation was likely caused by tyre load sensitivity: the cornering stiffness increases less than linearly as a function of the vertical load, while the custom tyre model assumes this relationship to be linear. The additional weight of the touring vs. the sports motorcycle led to an overestimated cornering stiffness increase. This hypothesis is corroborated by the fact that the relative error is higher at the front than at the rear, due to the more frontward centre of mass of the touring motorcycle compared to the other and due to the longitudinal load transfer produced by the braking action: in fact, when on the throttle (after $4.0\,\mathrm{s}$) the situation in terms of relative error reverses, as the load transfer changes sign. The previous work shows that in conditions of nominal static load and uncombined dynamics the slip angles follow those of the reference tyre almost perfectly. The slip ratios were correctly reproduced, even though the rider used both brakes. In contrast, in the characterisation manoeuvre, only one brake was used. This fact impacted each tyre's $F_z(s)$ relationship. However, the hypothesis, implicit in Equation (6a), that the additional load transfer (on top of the additional static load) does not significantly impact the longitudinal friction coefficient proved realistic. Tyre forces and moments were very close to those produced by the reference tyre model; the only exception was the rear

yaw moment: the fact that the tyre model overestimated it is coherent with the fact that the non-dimensional twisting stiffness used ($0.039\,\mathrm{m\,rad^{-1}}$) was higher than the true value ($0.031\,\mathrm{m\,rad^{-1}}$). Still, the description of the lateral forces is very close to the reference: the error on the yaw moments is small enough not to impact the lateral force distribution among the front and rear tyres. Even though the proposed tyre model is lenticular, while the Magic Formula tyre model uses a toroidal formulation, the front and rear overturning moments produced (computed by Equation (18)) were very close to the reference. Consequently, the roll angle (not shown) of the motorcycle employing the custom tyre model almost coincided with that of the reference. The fact that the single overturning moments, and not just their sum, were correctly reproduced constitutes a clear improvement over the previous formulation:[26] this was made possible by considering different front and rear non-dimensionalised overturning stiffnesses, each proportional to each tyre's width. The tyre model was developed by gradually adding features and checking the variation of the error of the signals: adding the combined slip formulation, the influence of the vertical weight and road friction, and the relaxation length, all improved the model's accuracy. This fact also testifies that the chosen manoeuvre did excite the corresponding phenomena to a sufficient degree.

The experimental characterisation showed that it was possible to estimate various signals relative to tyre behaviour (like the slip and camber angles, the slip ratios, and the forces produced by the tyre) using a real dataset and a limited set of straightforward sensors. As additional sensors (like wheel force transducers and slip angle sensors) were unavailable, comparing the estimated signals with the measured ones was not possible. However, the experimental characterisation showed the goodness of fit of the proposed functions and the results of the characterisation procedure. In particular, the tyre model correctly described the main aspects concerning tyre behaviour, like tyre load sensitivity (Figure 5b) and the slip angle being approximately null or towards the inside of the corner for small camber values (Figure 6). For higher lateral acceleration and thus camber angle values, the model predicted the slip angle to grow nonlinearly towards the outside of the corner. This result is coherent with the test bench data: the camber thrust alone becomes insufficient to produce the cornering force required for sufficiently high camber angle values, even when the camber stiffness reduction due to the slip angle is neglected. Moreover, the tyre model formulation was robust: the slip angle error predicted (Equation (41)) was smaller than that on the estimated non-dimensionalised corner and camber stiffnesses, in part due to the statistical approach used to derive the side force stiffness ratio $C$.

The validation of the tyre model concerning longitudinal dynamics showed a good description of the slip ratio for different levels of braking intensity: in the range of linear tyre behaviour, in the nonlinear range before the friction peak, and in the peak friction value too. Concerning lateral dynamics, the force produced by the tyre model was very similar to that measured at the test bench up to around $10°$, and close to it up to around $20°$. After that point, the error grew, and the model produced a lower lateral force than measured at the test bench: this phenomenon might be due to the machine track having possibly higher friction than the asphalt of the experimental tests. In fact, friction similarity predicts that the effect of road friction levels manifests when higher forces are demanded, while it does not impact tyre behaviour in the range of linear behaviour. Once again, the error on the results was lower than that on the coefficients, confirming the robustness of the model.

The experimental dataset has some limitations. The IMU used a standard GNSS system and not a differential GNSS. Due to the limited space available in the proving ground, the vehicle speed in the cornering phases was modest ($\sim 30\,\mathrm{km\,h^{-1}}$). Both factors increase the relative error on the estimated speed vector, that is used to compute the slip angles, which are at the basis of the estimation of the cornering stiffness and, consequently, the camber stiffness. While the characterisation results using a simulated dataset provided a lower bound to the estimation error, this relatively straightforward test should provide an upper bound to the error in reasonable testing conditions. The dataset did not employ wheel force transducers or slip angle sensors, which would have allowed a more thorough validation of the approach by comparing the measured and estimated signals. The test using the tyre test machine constituted a surrogate, allowing the comparison of some key aspects of lateral dynamics. A test employing a differential GNSS, executing manoeuvres at higher speeds, and employing sensors for the direct measurement of tyre forces and moment is, therefore, the next step to explore the potential and limitations of the approach. Lastly, due to the statistical approach used to derive some coefficients, the tyre model can produce a higher error concerning some quantities, like the yaw moment produced by the tyre. Simulations employing a realistic, physics-based tyre model would clarify further the error introduced by the assumptions used to reduce the number of unknowns. Future work could also assess characterising the tyre model using naturalistic riding data: it would introduce several external factors (like the road slope) compared to

a test in a controlled environment, which would need to be filtered out, but it would also provide a much more extensive and diverse dataset. Moreover, it would further reduce characterisation costs and allow cornering at higher speeds, which is beneficial for the slip angle estimation accuracy.

## Conclusion

An alternative formulation to the more classical magic formula for motorcycle tyres was proposed. It can be characterised using riding data employing a limited set of sensors and quasi-static, uncombined manoeuvres together with statistics from the literature. The formulation can describe transient, combined manoeuvres and is adaptive to different road friction and static load values, extending its validity. The tyre model describes not only the forces generated by the tyre but also more secondary aspects of tyre behaviour, like the moments generated along the longitudinal and vertical axes. The approach has been validated using a high-fidelity simulation environment and an experimental dataset, using data from an actual tyre bench test as the reference. Notably, a good description of the steering torque was achieved. The characterisation approach allows describing the exact tyres equipping the vehicle, with an implicit account of factors such as their inflation pressure, degree of wear, and the road state. The simplicity of the approach makes it possible for more subjects (research groups, suppliers) to obtain a realistic tyre model describing the tyres of a powered two-wheeler.

### Acknowledgements

The authors are grateful to the team that contributed to the execution of the test. In particular, they thank Cosimo Lucci for support in using the experimental bike and Simore Rosselli for the installation and calibration of the steering torque sensor.

### Funding

This research received no specific grant from any funding agency in the public, commercial, or not-for-profit sectors.

### Declaration of conflicting interests

The Authors declare that there is no conflict of interest.

### References

1. Lee H and Taheri S. Intelligent tires? A review of tire characterization literature. *IEEE Intelligent Transportation Systems Magazine* 2017; 9: 114–135. DOI:10.1109/mits.2017.2666584.
2. Hsu YJ, Laws SM and Gerdes JC. Estimation of tire slip angle and friction limits using steering torque. *IEEE Transactions on Control Systems Technology* 2010; 18(4): 896–907. DOI:10.1109/TCST.2009.2031099.
3. Bartolozzi M, Berzi L, Meli E et al. Similarities in steering control between cars and motorcycles: application to a low-complexity riding simulator. *Meccanica* 2022; 57(11): 2863–2883. DOI:10.1007/s11012-022-01603-8.
4. Sharp RS. The stability and control of motorcycles. *Archive: Journal of Mechanical Engineering Science 1959-1982 (vols 1-23)* 1971; 13: 316–329.
5. Cossalter V, Lot R and Massaro M. An advanced multibody code for handling and stability analysis of motorcycles. *Meccanica* 2010; 46: 943–958. DOI:https://doi.org/10.1007/s11012-010-9351-7.
6. Dell'Orto G, Ballo F, Gobbi M et al. Twisting torque – a simplified theoretical model for bicycle tyres. *Measurement* 2023; 221: 113460. DOI:10.1016/j.measurement.2023.113460.
7. Fujioka T and Goda K. Tire cornering properties at large camber angles: mechanism of the moment around the vertical axis. *JSAE Review* 1995; 16(3): 257–261. DOI:10.1016/0389-4304(95)00018-3.
8. Fujioka T and Goda K. Discrete brush tire model for calculating tire forces with large camber angle. *Vehicle System Dynamics* 1996; 25(sup1): 200–216. DOI:10.1080/00423119608969196.
9. Cossalter V, Doria A, Lot R et al. Dynamic properties of motorcycle and scooter tires: Measurement and comparison. *Vehicle System Dynamics* 2003; 39(5): 329–352. DOI:10.1076/vesd.39.5.329.14145.
10. Cossalter V and Doria A. The relation between contact patch geometry and the mechanical properties of motorcycle tyres. *Vehicle System Dynamics* 2005; 43(sup1): 156–164. DOI:10.1080/00423110500141045.
11. Romano L, Timpone F, Bruzelius F et al. Analytical results in transient brush tyre models: theory for large camber angles and classic solutions with limited friction. *Meccanica* 2022; 57(1): 165–191. DOI:10.1007/s11012-021-01422-3.
12. Pacejka HB. *Tire and vehicle dynamics*. Third ed. Oxford, United Kingdom: Butterworth-Heinemann, 2012.
13. Mottola M and Massaro M. Experimental estimation of the camber reduction factor of tyres. *Machines* 2022; 10(10). DOI:10.3390/machines10100921. URL https://www.mdpi.com/2075-1702/10/10/921.
14. Dugoff H, Fancher PS and Segel L. An analysis of tire traction properties and their influence on vehicle dynamic performance.

*SAE Transactions* 1970; 79: 1219–1243.

15. Massaro M, Mottola M, Bonisoli E et al. An experimental procedure for the identification of the dynamic parameters for the rigid-ring tyre model. *Meccanica* 2023; 58(5): 981–1001. DOI:10.1007/s11012-023-01654-5.
16. Gipser M. Ftire – the tire simulation model for all applications related to vehicle dynamics. *Vehicle System Dynamics* 2007; 45(sup1): 139–151. DOI:10.1080/00423110801899960.
17. Gallrein A and Bäcker M. Cdtire: a tire model for comfort and durability applications. *Vehicle System Dynamics* 2007; 45(sup1): 69–77. DOI:10.1080/00423110801931771.
18. de Vries EJ and Pacejka HB. Motorcycle tyre measurements and models. *Vehicle System Dynamics* 1998; 29(sup1): 280–298. DOI:10.1080/00423119808969565.
19. Higuchi A and Pacejka HB. The relaxation length concept at large wheel slip and camber. *Vehicle System Dynamics* 1997; 27(sup001): 50–64. DOI:10.1080/00423119708969644.
20. Cossalter V, Doria A, Giolo E et al. Identification of the characteristics of motorcycle and scooter tyres in the presence of large variations in inflation pressure. *Vehicle System Dynamics* 2014; 52(10): 1333–1354. DOI:10.1080/00423114.2014.940981.
21. Dell'Orto G, Ballo F, Mastinu G et al. Bicycle tyres – development of a new test-rig to measure mechanical characteristics. *Measurement* 2022; 202: 111813. DOI:10.1016/j.measurement.2022.111813.
22. Massaro M, Cossalter V and Cusimano G. The effect of the inflation pressure on the tyre properties and the motorcycle stability. *Proceedings of the Institution of Mechanical Engineers, Part D: Journal of automobile engineering* 2013; 227(10): 1480–1488.
23. Pacejka HB and Sharp RS. Shear force development by pneumatic tyres in steady state conditions: A review of modelling aspects. *Vehicle System Dynamics* 1991; 20(3-4): 121–175. DOI:10.1080/00423119108968983.
24. Lugo L, Bartolozzi M, Vandermeulen W et al. Test-driven full vehicle modelling for ADAS algorithm development. In *Symposium on International Automotive Technology*. SAE International. DOI:10.4271/2021-26-0033.
25. Fujii S, Shiozawa S, Shinagawa A et al. Investigation of steady-state cornering characteristics of motorcycles based on tire slip angle measurement. In *SAE Technical Paper*. SAE International. DOI:10.4271/2010-32-0105.
26. Bartolozzi M, Savino G and Pierini M. Novel high-fidelity tyre model for motorcycles to be characterised by quasi-static manoeuvres – rationale and numerical validation. *Vehicle System Dynamics* 2022; 60(12): 4290–4316. DOI:10.1080/00423114.2021.2013506.
27. Road vehicles - vehicle dynamics and road-holding ability - vocabulary. Standard, International Organization for Standardization, 2011.
28. Bakker E, Pacejka HB and Lidner L. A new tire model with an application in vehicle dynamics studies. *SAE transactions* 1989; 98: 101–113.
29. Guiggiani M. *The Science of Vehicle Dynamics: Handling, Braking, and Ride of Road and Race Cars*. Third ed. Springer, 2022. DOI:10.1007/978-3-031-06461-6.
30. Lot R. A motorcycle tire model for dynamic simulations: Theoretical and experimental aspects. *Meccanica* 2004; 39: 207–220. DOI:10.1023/B:MECC.0000022842.12077.5c.
31. Cossalter V, Doria A and Lot R. Steady turning of two-wheeled vehicles. *Vehicle System Dynamics* 1999; 31: 157–181. DOI:10.1076/vesd.31.3.157.2013.
32. Cossalter V. *Motorcycle Dynamics*. Second ed. Raleigh, North Carolina: Lulu.com, 2006.
33. Sharp RS, Evangelou S and Limebeer DJN. Advances in the modelling of motorcycle dynamics. *Multibody System Dynamics* 2004; 12: 251–283. DOI:10.1023/B:MUBO.0000049195.60868.a2.
34. Teerhuis AP and Jansen ST. Motorcycle state estimation for lateral dynamics. *Vehicle System Dynamics* 2012; 50(8): 1261–1276. DOI:10.1080/00423114.2012.656655.
35. Mechanical Simulation Corporation. BikeSim [Internet], 2023. Cited Jul 23. Available from: https://www.carsim.com/products/bikesim/.
36. Cossalter V and Sadauckas J. Elaboration and quantitative assessment of manoeuvrability for motorcycle lane change. *Vehicle System Dynamics* 2006; 44(12): 903–920. DOI:10.1080/00423110600742072.
37. Hisaoka Y, Yamamoto M and Okada A. Closed-loop analysis of vehicle behavior during braking in a turn. *JSAE Review* 1999; 20(4): 537–542. DOI:10.1016/S0389-4304(99)00042-9.
38. Holland PW and Welsch RE. Robust regression using iteratively reweighted least-squares. *Communications in Statistics - Theory and Methods* 1977; 6(9): 813–827. DOI:10.1080/03610927708827533.
39. Bartolozzi M, Savino G and Pierini M. Motorcycle steering torque estimation using a simplified front assembly model: experimental validation and manoeuvrability implications. *Vehicle System Dynamics* 2023; DOI:10.1080/00423114.2023.2194542.
40. Cossalter V, Lot R, Massaro M et al. Investigation of motorcycle steering torque components. *AIP Conference Proceedings* 2011; 1394: 35–46. DOI:10.1063/1.3649934.

# Appendix

## Notation

### Quantities

| | |
|---|---|
| $b$, $c$, $d$, $e_1$, $e_2$ | Magic Formula coefficients |
| c | generic coefficient |
| $c_{\text{drag}}$ | drag resistance coefficient |
| $c_{\text{rol}}$ | dimensionless rolling resistance coefficient |
| $C$ | side force stiffness ratio |
| $F_x$, $F_y$, $F_z$ | longitudinal, lateral and vertical force |
| $F_{x0}$, $F_{y\alpha 0}$ | slip force base curves |
| $F^*_{x0}$, $F^*_{y\alpha 0}$ | anisotropic slip force base curves |
| $g$ | gravity of Earth |
| $h_G$ | centre of gravity height |
| $k_t$, $k_x$, $k_\alpha$, $k_\gamma$ | non-dimensionalised twisting, overturning, cornering, and camber stiffnesses |
| $k_{\alpha 0}$, $k_{\gamma 0}$ | non-dimensionalised cornering and camber stiffnesses for vanishing slip and camber |
| $K_z$, $K_\alpha$, $K_\gamma$ | vertical, cornering, and camber stiffness |
| $l$ | wheelbase |
| $m$ | mass |
| $M_x$, $M_z$ | longitudinal and yaw moments |
| $\mathrm{q}_1$ | slip transition coefficient |
| $r_{\text{l}}$ | relaxation length |
| $r_{\text{f}}$, $r_{\text{r}}$ | front and rear tyre width |
| $R_{\text{rol}}$, $R_{\text{unl}}$, $R_{\text{loa}}$ | rolling, unloaded, and loaded wheel radii |
| $s$ | slip ratio |
| $t$ | time |
| $t_{\text{p}}$, $t_{\text{p0}}$ | pneumatic trail with and without slip |
| $v$ | speed |
| $\alpha$ | slip angle |
| $\delta$ | steering angle |
| $\epsilon$ | caster angle |
| $\Gamma$ | anisotropy transition variable |
| $\eta$ | normalised slip direction |
| $\theta$ | slip direction |
| $\lambda$ | slip force direction |
| $\mu$, $\mu_0$ | actual and reference road friction coefficient |
| $\mu_x$, $\mu_y$ | longitudinal and lateral friction coefficient |
| $\rho$ | brake balance |
| $\sigma$ | theoretical slip |
| $\tau$ | steering torque |
| $\phi$, $\dot{\phi}$ | roll angle and roll rate |
| $\phi_{\text{len}}$ | lenticular tyres steady-state roll angle |
| $\dot{\psi}$ | yaw rate |
| $\omega$ | wheel angular speed |

### Superscripts

| | |
|---|---|
| max | relative to maximum |
| tot | total |
| unc | uncombined |
| $'$ | equivalent slip |
| $^*$ | normalised slip |
| $\hat{}$ | tyre slip force function |

### Subscripts

| | |
|---|---|
| kin | kinematic |
| s | slip |
| tan | tangential |
| $x, y, x$ | relative to the longitudinal, lateral, and vertical direction |
| f,r | relative to the front and rear tyre |

### Other

| | |
|---|---|
| $\langle\cdot\rangle$ | tyre model function argument |